

**Cooperative nucleation modes in polycrystalline CoxPd1-x nanowires**

M. S. Viqueira, G. Pozo-López, S. E. Urreta, A. M. Condó, D. R. Cornejo, and L. M. Fabietti

Citation: *Journal of Applied Physics* **117**, 204301 (2015); doi: 10.1063/1.4921700

View online: <http://dx.doi.org/10.1063/1.4921700>

View Table of Contents: <http://scitation.aip.org/content/aip/journal/jap/117/20?ver=pdfcov>

Published by the **AIP Publishing**

---

**Articles you may be interested in**

[Gradient magnetic binary alloy nanowire](#)

*J. Appl. Phys.* **115**, 17B514 (2014); 10.1063/1.4864248

[Structural and magnetic characterization of as-prepared and annealed FeCoCu nanowire arrays in ordered anodic aluminum oxide templates](#)

*J. Appl. Phys.* **115**, 133904 (2014); 10.1063/1.4870289

[Enhanced magnetic performance of metal-organic nanowire arrays by FeCo/polypyrrole co-electrodeposition](#)

*J. Appl. Phys.* **113**, 17B908 (2013); 10.1063/1.4800835

[Effect of external magnetic field on magnetic properties of Co-Pt nanotubes and nanowires](#)

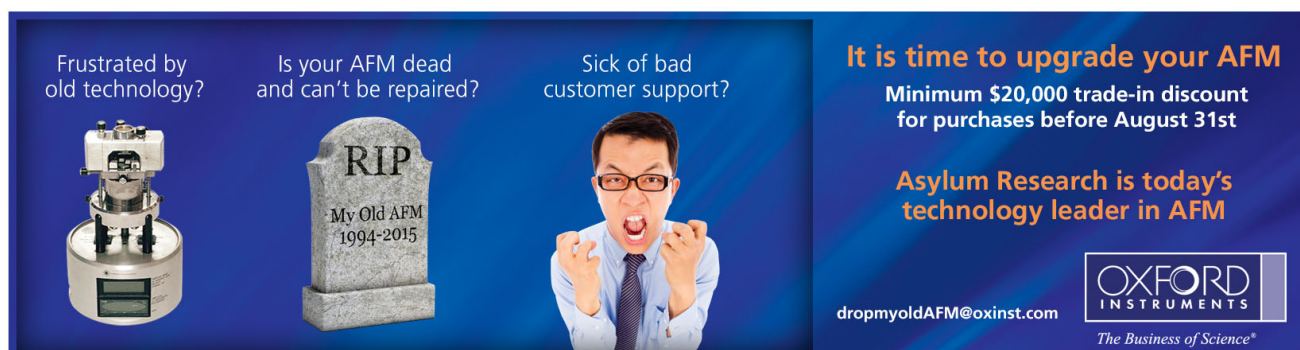
*J. Appl. Phys.* **109**, 07E157 (2011); 10.1063/1.3565205

[Electrochemical fabrication and magnetization properties of CoCrPt nanowires and nanotubes](#)

*Appl. Phys. Lett.* **94**, 203101 (2009); 10.1063/1.3139059

---

Frustrated by old technology?      Is your AFM dead and can't be repaired?      Sick of bad customer support?



**It is time to upgrade your AFM**  
Minimum \$20,000 trade-in discount for purchases before August 31st

**Asylum Research is today's technology leader in AFM**

dropmyoldAFM@oxinst.com

**OXFORD INSTRUMENTS**  
*The Business of Science®*

## Cooperative nucleation modes in polycrystalline $\text{Co}_x\text{Pd}_{1-x}$ nanowires

M. S. Viqueira,<sup>1,2</sup> G. Pozo-López,<sup>1,2,3</sup> S. E. Urreta,<sup>1,a)</sup> A. M. Condó,<sup>3,4</sup> D. R. Cornejo,<sup>5</sup> and L. M. Fabietti<sup>1,2,3</sup>

<sup>1</sup>Facultad de Matemática, Astronomía y Física, Universidad Nacional de Córdoba, Ciudad Universitaria, 5000 Córdoba, Argentina

<sup>2</sup>Instituto de Física Enrique Gaviola – CONICET, FAMAFA, Ciudad Universitaria, 5000 Córdoba, Argentina

<sup>3</sup>Consejo Nacional de Investigaciones Científicas y Técnicas (CONICET), Argentina

<sup>4</sup>Centro Atómico Bariloche, Comisión Nacional de Energía Atómica – Instituto Balseiro, Universidad Nacional de Cuyo, Av. Bustillo 9500, 8400 San Carlos de Bariloche, Argentina

<sup>5</sup>Instituto de Física, Universidade de São Paulo, 05508-900 São Paulo, São Paulo, Brazil

(Received 5 January 2015; accepted 14 May 2015; published online 28 May 2015)

Polycrystalline  $\text{Co}_x\text{Pd}_{1-x}$  ( $x = 1, 0.60, 0.45, 0.23,$  and  $0.11$ ) cylindrical nanowires ( $\phi = 18\text{--}35$  nm, about  $1\ \mu\text{m}$  length) are produced by AC electrodeposition into hexagonally ordered alumina pores. Single-phase nanowires of an *fcc* Co-Pd solid solution, with randomly oriented equiaxed grains ( $7\text{--}12$  nm) are obtained; in all the cases, the grain size is smaller than the wire diameter. The coercive field and the reduced remanence of Co-rich nanowire arrays are hardly sensitive to temperature within the range varying from 4 K to 300 K. On the other hand, in Pd-rich nanowires both magnitudes are smaller and they largely increase when cooling below 100 K. This behavior also depends on the mean grain size. These facts are systematized considering two main aspects: the non-trivial temperature and composition dependence of the crystalline anisotropy and the saturation magnetostriction in Co-Pd alloys; and a random anisotropy effect, which defines a nucleation localization length that may involve more than a single grain, and thus promotes more cooperative nucleation modes. © 2015 AIP Publishing LLC. [<http://dx.doi.org/10.1063/1.4921700>]

### I. INTRODUCTION

Magnetization reversal mechanisms in ferromagnetic nanowires have been thoroughly investigated.<sup>1–9</sup> Unlike isolated nanowires,<sup>1</sup> arrays exhibit non-square hysteresis loops. This is attributed to the size/shape distribution in the sample and to magnetic interactions among the nanowires in the array.<sup>10–13</sup> In fact, the hysteresis loop shape is determined by the interplay between the effective anisotropy field of individual nanowires, and the dipolar interaction fields of the array as a whole. This dipolar coupling is often described in a mean field approximation by an additional uniaxial anisotropy, favoring an in-plane easy axis. For planar regular arrays of magnetic nanowires, this dipolar demagnetizing field becomes  $\mu_0 H_{\text{dip}} = -P J_S$ ,<sup>10</sup> where  $J_S$  is the saturation polarization and  $P$ , the template porosity.

For short, single crystalline wires with a quite low aspect ratio  $a_r$  ( $=L/D$ , with  $L$  and  $D$  the wire length and diameter, respectively), two *de-localized* (that is, involving all the wire volume) switching modes—coherent rotation and curling—are observed, while *localized* magnetization reversal modes are predicted for long and wide nanowires.<sup>2,3</sup> In long cylinders with uniform structure, polarization reversal takes place by the nucleation and propagation of a single domain wall,<sup>1,7–9</sup> this wall preferentially nucleating at the wire ends. Depending on the radius and on the nanowire material, the magnetization reversal may proceed by the nucleation/propagation of either a vortex domain wall or a transverse wall, which move at very high velocities along the entire wire.

These models, involving nucleation and the further free expansion of a single, ideal domain wall through the wires, may be rigorously valid for single crystalline wires, and they may be further adapted to individual grains in cases where the mean grain size is quite large as compared with the domain wall size and the wire diameter. However, in polycrystalline wires with a relatively small grain size, reversal is likely to initiate at the morphological inhomogeneities. Single-crystalline wires exhibit a weak localization of the nucleation mode while structural inhomogeneities in polycrystalline nanowires tend to localize it. Grain boundaries, fluctuations in the wire thickness, atomic defects, grain misalignment, and/or geometrical features at the wire ends—see Figures 2–5—promote a strong localization of the nucleation mode.<sup>2,3</sup> In addition, in wires with low saturation magnetization and a small grain size, the competition between interatomic exchange and anisotropy may also produce random-anisotropy effects, which further reduce the coercivity.

In polycrystalline nanowires, the angular dependence of coercivity seems to be controlled by coherent rotation or curling in a volume even smaller than the grain size  $d_G$ . For example, Wegrowe *et al.*<sup>14</sup> report in Ni nanowires that the angular dependence of the magnetoresistance may only be quantitatively explained by the usual anisotropic magnetoresistance model, if the nucleation volume is assumed to be a “rugby ball,” 50 times smaller than the whole wire, and with a nucleus aspect ratio  $a_r^* \approx 2$ . This is a very small value considering that Ni wires have  $a_r = 100$ . Magnetic viscosity measurements<sup>15</sup> lead to quite small activation volumes for polarization reversal, indicating that thermally activated magnetization processes are controlled by the localized nucleation

<sup>a)</sup>Author to whom correspondence should be addressed. Electronic mail: [urreta@famaf.unc.edu.ar](mailto:urreta@famaf.unc.edu.ar)

of an inverse domain surrounded by a wall-like spin configuration. At the coercive field, at room temperature, activation volume values of about  $(11.5 \text{ nm})^3$ ,  $(12.8 \text{ nm})^3$ , and  $(18 \text{ nm})^3$  are reported<sup>15</sup> for Fe ( $D=9 \text{ nm}$ ;  $d_G=40 \text{ nm}$ ,  $L=1 \mu\text{m}$ ), Co ( $D=20 \text{ nm}$ ;  $L=1 \mu\text{m}$ ), and Ni ( $D=18 \text{ nm}$ ;  $d_G=10 \text{ nm}$ ,  $L=1 \mu\text{m}$ ) nanowires, respectively. Thus, in polycrystalline nanowires, *localized* coherent rotation or *localized* curling should be considered as nucleation mechanisms.

In magnetically hard polycrystalline nanowires ( $K_C \gg J_0^2/\mu_0^2$ ), a random anisotropy effect may appear when the domain wall parameter in the material  $\delta_w (= \sqrt{A/K_C}$ , with  $A$  the exchange and  $K_C$  the magnetocrystalline anisotropy constants) is larger than the crystallite size  $d_G$  in the wire. This inter-granular interaction defines a nucleation localization length, which may involve more than a single grain, making the nucleation mode cooperative.<sup>2</sup> In magnetically semi-hard and soft polycrystalline nanowires, magnetostatic surface charges (and local stray fields) may reduce the role of the polycrystalline anisotropy. Thus,  $K_C$  is often replaced by an effective uniaxial anisotropy constant  $K_{\text{eff}}$  containing in general magnetocrystalline, shape and magneto-elastic contributions.<sup>15,16</sup> In the case of predominant shape anisotropy, the domain wall parameter  $\delta_w^*$  scales the exchange length  $L_{\text{ex}} (= \sqrt{2A\mu_0/J_S^2})$ . Skomski *et al.*<sup>2</sup> provide a qualitative understanding of the nucleation localization phenomenon, ruled by the sample's polycrystalline nature, in a mechanism/localization map or phase diagram, involving magnetic and structural characteristic lengths. In addition, different regimes and nucleation modes are proposed.

In this article, the composition and temperature dependence of the coercive properties of single-phase *fcc*  $\text{Co}_x\text{Pd}_{1-x}$  nanowire arrays, with small grain size and similar geometry and aspect ratio, is discussed. Grain size and composition are considered to explain the temperature dependence of the coercive field and the relative remanence in Pd-rich wires below 100 K. The observed behaviors are attributed to changes in the effective uniaxial anisotropy along the wires, given by the interplay between magnetostatic, magnetoelastic, and magnetocrystalline energies in the array.

Shape anisotropy (growing with the saturation polarization) should not be regarded as the only responsible for the magnetic hardening observed in CoPd nanowires at temperatures below 100 K. It is also necessary to consider a transition from a regime in which the magnetostatic energy determines the spin configuration in the sample at 300 K, to another one, in which this configuration becomes defined by the crystalline anisotropy. This transition may change the nucleation localization length. The increments in coercivity and remanence values observed at low temperature in Pd-rich wires (with a lower shape anisotropy) are, therefore, explained taking into account that the crystalline anisotropy becomes dominant, it determines local spin configurations and promotes different nucleation regimes and less cooperative nucleation modes.

## II. EXPERIMENTAL PROCEDURE

$\text{Co}_x\text{Pd}_{1-x}$  nanowires were prepared by electrodepositing the metal ions within the 20–30 nm nominal diameter pores

of an anodized aluminum oxide (AAO) membrane,<sup>17</sup> which acted as a hard template. The template porosity  $P$  is estimated as  $P = (\pi/2\sqrt{3})(D/D_{\text{int}})^2$ , with  $D$  as the nanowire diameter, and  $D_{\text{int}}$  as the mean centre-to-centre inter-pore distance in the array. The resulting values are similar in all the samples,  $P = (0.11 \pm 0.01)$  in good agreement with the 10%-porosity law.<sup>18</sup>

The electrodeposition of Co-Pd nanowires with different compositions was carried out in aqueous electrolytic baths (keeping pH=5) with different proportions of  $\text{CoCl}_2$  and  $\text{PdCl}_2$ , containing variable relations of  $\text{Co}^{2+}$  and  $\text{Pd}^{2+}$  ions, and 30 g/l of  $\text{H}_3\text{BO}_4$ , which were added to enhance conductivity. The electrodeposition of CoPd nanowires was performed for a few minutes at 295 K, under a sinusoidal wave of 200 Hz and 25  $V_{\text{rms}}$ . A two-electrode electrochemical cell was used, where the remaining Al in the AAO template served as a working electrode, and a graphite rod as an auxiliary one.

The morphology and microstructure of the resulting samples were investigated by scanning electron microscopy (SEM) in a FE-SEM Sigma Zeiss instrument, and by transmission electron microscopy (TEM) in a Philips CM200UT microscope, operating at 200 kV. X-ray diffractograms were measured in a Philips PW 3830 X-ray diffractometer (XRD) with Cu-K $\alpha$  radiation ( $\lambda = 1.5418 \text{ \AA}$ ), in the Bragg-Brentano configuration. For each nanowire array produced, the global composition was first determined by energy-dispersive X-ray spectroscopy (EDS) techniques in a JEOL JXA-8230 Electron Probe Microanalyzer and further confirmed for each individual sample in the TEM. The values obtained were statistically indistinguishable within  $\pm 4$  at. % Co. Samples for TEM observations were prepared by dispersing the liberated nanowires in ethanol and then, depositing a drop of this emulsion on a holey carbon-coated copper grid.

Magnetic properties were characterized by measuring the hysteresis loops in a MPMS (Magnetic Properties Measurement System) Quantum Design SQUID magnetometer, in the temperature range between 5 K and 300 K. Loops were measured at two different relative orientations between the sample and the applied magnetic field:  $\phi = 0^\circ$  (PA, with the magnetic field parallel to the long nanowire axis) and  $\phi = 90^\circ$  (PE, with the magnetic field perpendicular to the long nanowire axis). The different Co-Pd arrays were named CoX, being X the Cobalt composition in at. %.

## III. RESULTS AND DISCUSSION

### A. Morphology and structure

The main characteristics of the metallic nanowires are listed in Table I. The mean wire length was controlled by the electrodeposition time, reaching values of  $L = (1.0 \pm 0.2) \mu\text{m}$  with a mean aspect ratio  $a$ , close to 40 in all cases.

Figure 1 shows the X-ray diffraction patterns corresponding to the arrays Co60 and Co11, measured after removing the aluminum substrate. The narrow peak at  $31.66^\circ$  corresponds to the polystyrene layer (JCPDS card No. 00-0130836) deposited onto the alumina membrane to improve its mechanical resistance. The lines at  $40.12^\circ$  and  $46.66^\circ$  are indexed as the (111) and the (200) peaks of a *fcc* Pd (JCPDS card No. 00-046-1043). The pattern corresponding to Co100 nanowires,

TABLE I. Morphology and microstructure corresponding to the different samples considered; mean grain size  $d_G$ , and diameter  $D$  resulting from fitting the respective histograms by a lognormal distribution (correlation factor  $r^2 > 0.993$ ) and mean wire length  $L$ , determined by TEM. The demagnetizing factor  $N_{\parallel}$  parallel to the wire long axis, estimated following Ref. 19, is also quoted.

Sample	$d_G$ (nm)	$L$ ( $\mu\text{m}$ )	$N_{\parallel}$	$D$ (nm)
Co	$42 \pm 8$	$0.8 \pm 0.1$	0.0105	$18 \pm 2$
Co60	$7.5 \pm 0.5$	$1.2 \pm 0.2$	0.0193	$28 \pm 5$
Co45	$11.5 \pm 0.5$	$1.0 \pm 0.2$	0.0084	$30 \pm 2$
Co23	$11.5 \pm 0.5$	$1.0 \pm 0.2$	0.0085	$18 \pm 4$
Co11	$8.5 \pm 0.5$	$1.0 \pm 0.2$	0.0085	$26 \pm 5$

exhibiting a marked (001) hexagonal texture is also shown as reference in Figure 1. TEM results confirm that all the wires with intermediate Co content are single-phase, a disordered solid solution Pd(Co) with a cubic (*fcc*) crystalline structure (as observed in the X-ray diffraction diagram).

From TEM results, the structure parameters for all the samples were determined and their values listed in Table I. Figures 2–5 depict Co60, Co45, Co23, and Co11 nanowires, respectively.

As mentioned before, electron diffraction patterns indicate that the wires are single phase, a *fcc* Pd(Co) alloy, in agreement with XRD results. The small grains are equiaxed and randomly oriented; the addition of Pd to Co wires reduces the grain size. However, no clear correlation could be established between the grain size and the alloy composition nor with the nanowire diameter. Nanowires exhibit fluctuations in diameter, severe irregularities at the ends and

rough surfaces, as illustrated in Figures 2–5. These features are likely to promote *localized* demagnetization modes.<sup>2,3</sup>

## B. Temperature dependent hysteresis properties

The temperature dependence of the hysteresis properties and the effect of thermal activation on the coercivity mechanism in the CoPd nanowire arrays were investigated. DC magnetization versus temperature curves were measured, following the conventional zero field cooling (ZFC) and field cooling (FC) protocols, in the PA configuration, under an applied field of 10 mT. These magnetization measurements provide an estimation of the effective blocking temperature distribution for magnetization reversal,<sup>20</sup> related to the activation barrier distribution in the sample.

The resulting relative values ( $J(T)/J(300\text{ K})$ ) have been plotted in Figure 6(a) for Co11, Co23, Co45, and Co60 arrays. In the ZFC-FC curve, two characteristic temperatures are distinguished: the mean blocking temperature  $T_B$ , at which the ZFC curve exhibits a local maximum, and the irreversibility temperature  $T_{irr}$ , where the ZFC and FC curves bifurcate.

In our systems, in which exchange, crystalline and magnetostatic interactions are present, the blocking temperature  $T_B$  may be regarded as the temperature below which a given volume or magnetic grain does not reverse its magnetization by a thermally activated nucleation mechanism, during the time scale of the measurement. On the other hand, the irreversibility temperature  $T_{irr}$  indicates the onset of blocking of the magnetically harder volumes in the sample. The difference between  $T_{irr}$  and  $T_B$  provides a qualitative measure of the blocking temperature distribution width.

The ZFC curves corresponding to the Co11 and Co23 arrays show a clear and broad maximum below room temperature. This maximum can also be observed (though less defined) in the Co45 and Co60 samples. Co11 arrays show  $T_{irr}$ , below 300 K in agreement with the quite low coercivity of these samples, whereas for the other three alloys  $T_{irr}$  is above 300 K.

The derivative plots  $d(J_{ZFC} - J_{FC})/dT$  vs.  $T$  curves corresponding to samples in Figure 6(a), measured in the easy PA configuration, are displayed in Figure 6(b). The curve corresponding to Co11 monotonically decreases, and becomes nearly zero at 260 K (which is identified as  $T_{irr}$  of this sample). This indicates that the magnetic polarization inversion mechanism is completely activated at 300 K. The curves corresponding to the other three samples show a well-marked maximum. Then, they pass through a minimum, and further on grow until the maximum temperature (300 K) is reached, as if another maximum were present at higher temperature. Measurements at temperatures above 300 K are necessary to confirm this latter hypothesis. A quite similar behavior is observed in both, PA and PE configurations as illustrated in the inset of Figure 6(b). On the one hand, it is noticed that the distribution maximum shifts to higher temperatures (harder nucleation modes) when the Co content increases. On the other hand, it decreases to lower temperatures when the mean grain size diminishes, as illustrated by

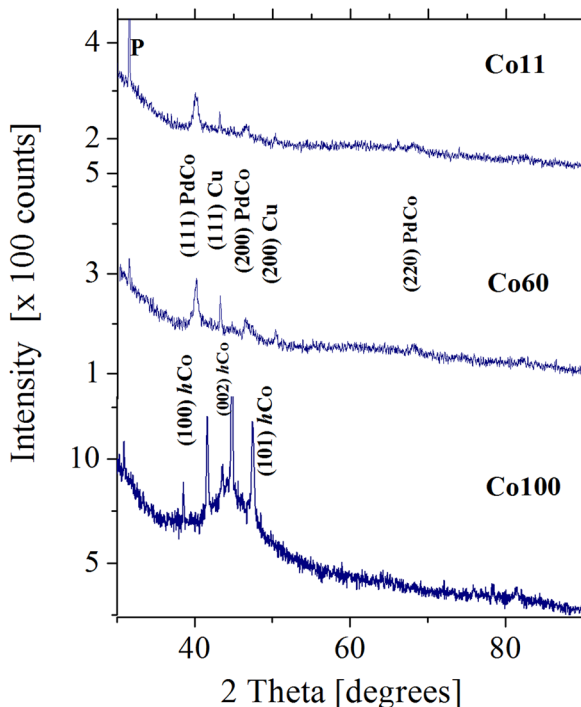


FIG. 1. XRD patterns corresponding to Co11, Co60, and Co100 arrays, after removal of the Al substrate. The reflection denoted by P arises from the polystyrene layer deposited to improve the membrane mechanical resistance. Small Cu crystals, originated in the Al dissolution process are also detected.

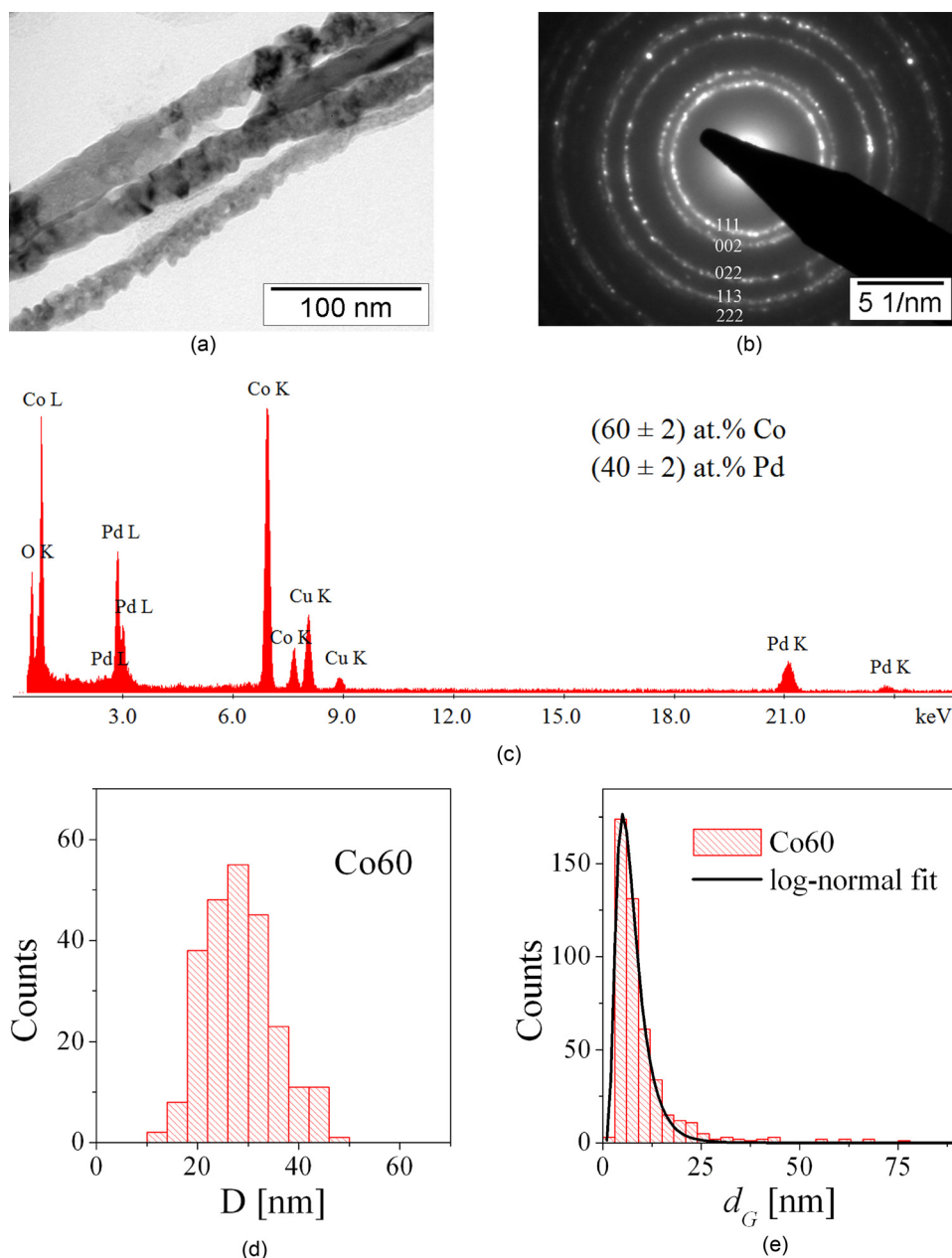


FIG. 2. (a) Bright field (BF) TEM micrograph of Co60 polycrystalline nanowires, with quite a small grain size. (b) Electron diffraction pattern, (c) EDS spectrum, (d) diameter  $D$ , and (e) grain size  $d_G$  histograms, resulting from TEM data.

the curves corresponding to the samples Co45 ( $d_G = 11.5$  nm) and Co60 ( $d_G = 7.5$  nm) in Figure 6(b).

The temperature dependence of the coercive field  $\mu_0 H_C$  and the squareness factor  $S = J_R/J_S$  of the Co60, Co45, Co23, and Co11 nanowire arrays are shown in Figure 7. The coercive field and the relative remanence of Co and Co-rich arrays (Co60 and Co45) remain almost temperature independent, exhibiting only small slopes in the range of 4 K–300 K, as expected for shape anisotropy controlled switching fields. No transition from a shape to crystalline anisotropy controlled coercivity was observed in these samples. The squareness of the loop in the PA configuration slightly decreases, while it lightly increases during cooling for the PE direction. This indicates rather small changes in the effective anisotropy in the parallel and the perpendicular directions during cooling.

When the Pd content increases above 55 at. %, the coercive field and the squareness become more temperature sensitive, as if larger magnetoelastic and/or magnetocrystalline contributions were also present in the effective anisotropy. In fact, the magnetocrystalline anisotropy energy  $K_C$ <sup>21</sup> and the saturation magnetostriction  $\lambda_S$ <sup>22,23</sup> of CoPd alloys depend significantly on composition and temperature. Both constants are negative and they go through a maximum absolute value between 10 and 25 at. % Co, and at temperatures below 100 K. Data for  $K_C$ ,  $\lambda_S$ , and  $J_S$  corresponding to 4 K and 300 K, taken from previous works of Bozorth *et al.*,<sup>21</sup> Fujiwara *et al.*,<sup>22</sup> and Takahashi *et al.*<sup>23</sup> are listed in Table II, together with the main magnetic lengths at these temperatures. The Young's modulus  $E$  and the exchange energy constant  $A$  for each composition are roughly estimated using the mixture rule.

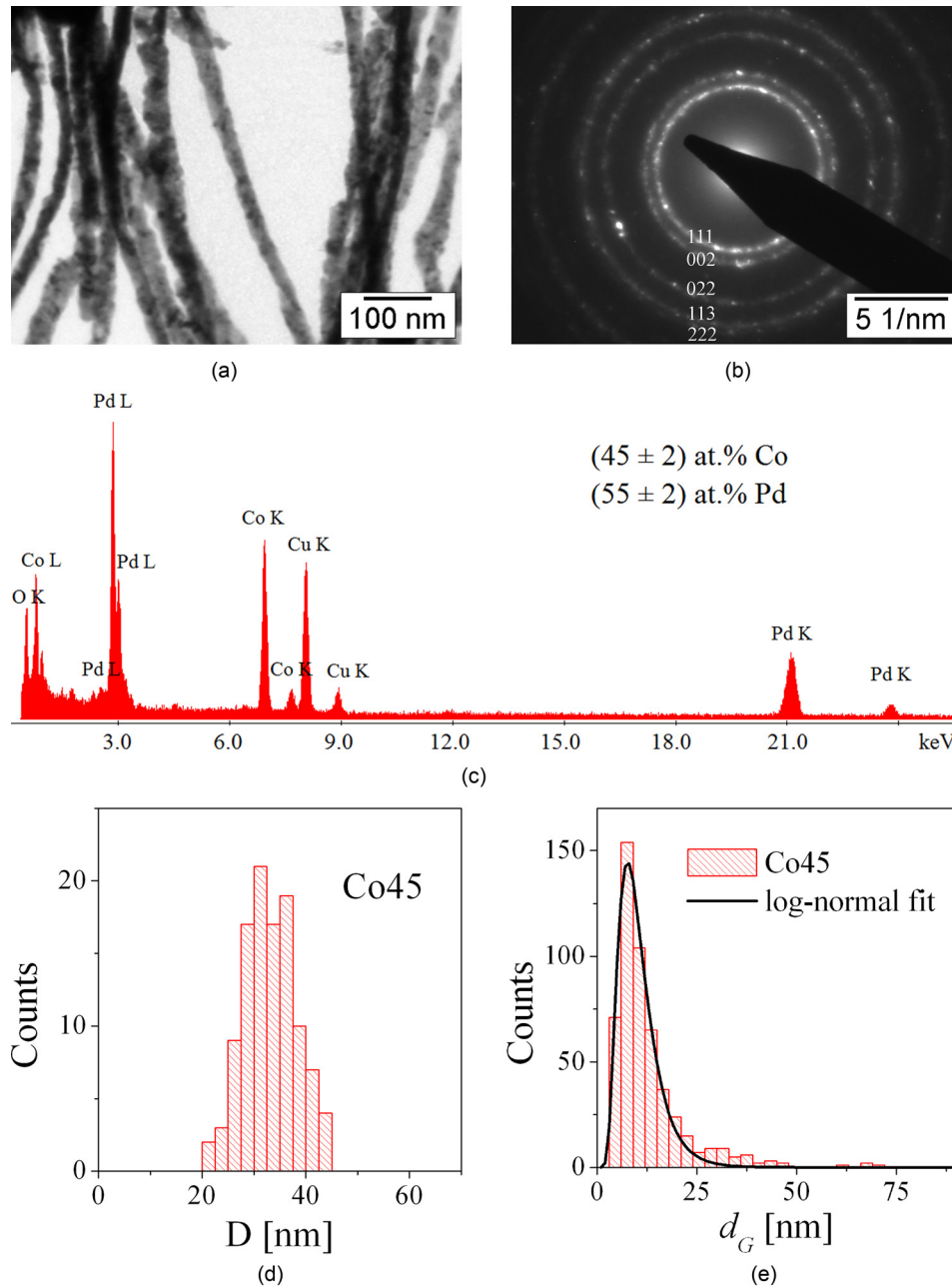


FIG. 3. (a) Bright field (BF) TEM micrograph of Co45 polycrystalline nanowires. (b) Electron diffraction pattern, (c) EDS spectrum, (d) diameter  $D$ , and (e) grain size  $d_G$  histograms, resulting from TEM data.

It is worth noting that the mean nanowire diameters satisfy  $D \cong D_{coh} = 7.3 \sqrt{\mu_0 A / J_S^2}$  with values of  $D_{coh}$  between 18 nm (Co100) and 25 nm (Co11). Then, localized nucleation at imperfections is expected to control the magnetization reversal process.

### C. Magnetic anisotropy

The magnitude of the coercive field in these small-grained nanowires is related to an effective magnetic anisotropy resulting from magnetocrystalline, magnetoelastic, and magnetostatic (shape) anisotropies and from the dipolar interaction field  $\mu_0 H_{dip}$ . Assuming that this effective anisotropy is uniaxial (parallel to the wire length), the effective anisotropy field becomes<sup>24</sup>

$$\mu_0 H_{eff}^A = \mu_0 H_{sh} + \mu_0 H_{\lambda} + \mu_0 H_K. \quad (1)$$

An upper bound for the shape anisotropy field is approximately given by  $\mu_0 H_{sh} = (N_{\perp} - N_{\parallel}) J_S$ , where  $(N_{\perp} - N_{\parallel})$  is the difference between the demagnetizing factors of a homogeneous cylinder, corresponding to the longitudinal ( $N_{\parallel}$ ) and transversal ( $N_{\perp}$ ) directions. These anisotropy field values are listed in Table III for arrays with different compositions at 4 K and 300 K. As mentioned above, actual values in polycrystalline wires may be smaller than this upper bound due to local stray fields. Then, it may be concluded that the shape anisotropy is dominant in Co and Co60 wires at all temperatures, but other contributions become important in Pd-rich wires, especially below room temperature.

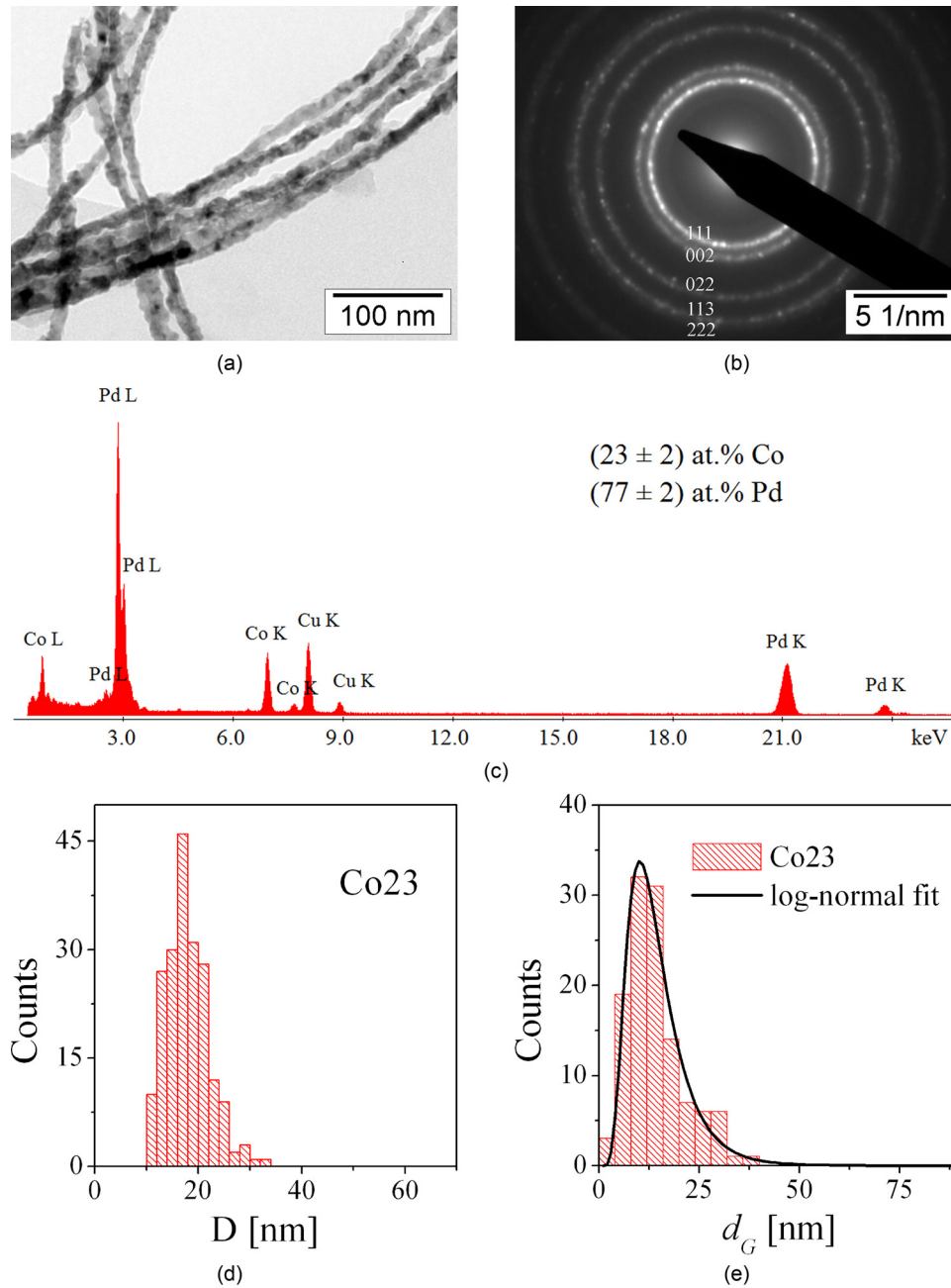


FIG. 4. (a) Bright field (BF) TEM micrograph of Co23 nanowires. (b) Electron diffraction pattern, (c) EDS spectrum, (d) diameter  $D$ , and (e) grain size  $d_G$  histograms, resulting from TEM data.

At low temperature, a magnetoelastic anisotropy field arising from the thermal expansion mismatch between the aluminum substrate, the alumina template, and the metallic nanowires, should be considered.<sup>25</sup> Assuming that the lateral contraction of the alumina template and the reduction of the pore diameter are only controlled by the contraction of the Al substrate, the alumina contraction in the direction PE is  $\epsilon_{alumina}^{PE} = (\alpha_{Al} - \alpha_{alumina}) \Delta T = -4.45 \times 10^{-3}$  ( $\alpha_{Al} = 23.8 \times 10^{-6}$ ;  $\alpha_{alumina} = 6 \times 10^{-6}$ ;  $\Delta T = -295 K$ ).

The elongation of the alumina pore then becomes  $\epsilon_{alumina}^{PA} = -\nu_{alumina} \epsilon_{alumina}^{PE} = 1.02 \times 10^{-3}$  ( $\nu_{alumina} = 0.23$ ). Because of the mismatch between the Al support and the CoPd wire, this latter undergoes an axial extension  $\epsilon_{CoPd}^{PA} = -\nu_{CoPd} \epsilon_{CoPd}^{PE}$  ( $\nu_{CoPd} = 0.3$ ), which is slightly smaller than

that of the alumina pore. Then, assuming a perfect adhesion (keeping the wires perfectly attached to the template,  $\epsilon_{CoPd}^{PA} = \epsilon_{alumina}^{PA}$ ), an upper limit for the tensile stress is given by:  $\sigma_{CoPd}^{PA} = E_{CoPd} \epsilon_{CoPd}^{PA} = 158 \text{ MPa}$  (Co11) and 195 MPa (Co45). This stress introduces an extra axial effective field  $\mu_0 H_{\sigma}^{CoPd}(4K) = 3\mu_0 \lambda_S \sigma_{CoPd}^{PA} / J_S \cong -159 \text{ mT}$  (Co11) and 63 mT (Co45) at 4 K, which reduces the shape anisotropy along the nanowire axis.

Finally, the magnetocrystalline anisotropy field,  $\mu_0 H_K = 2\mu_0 K_C / J_S$ , is also estimated as a function of the alloy composition at the two temperatures. This field, the corresponding magnetoelastic and magnetocrystalline anisotropy fields (estimated with data from Refs. 21–23), and the measured coercive fields are quoted in Table III.

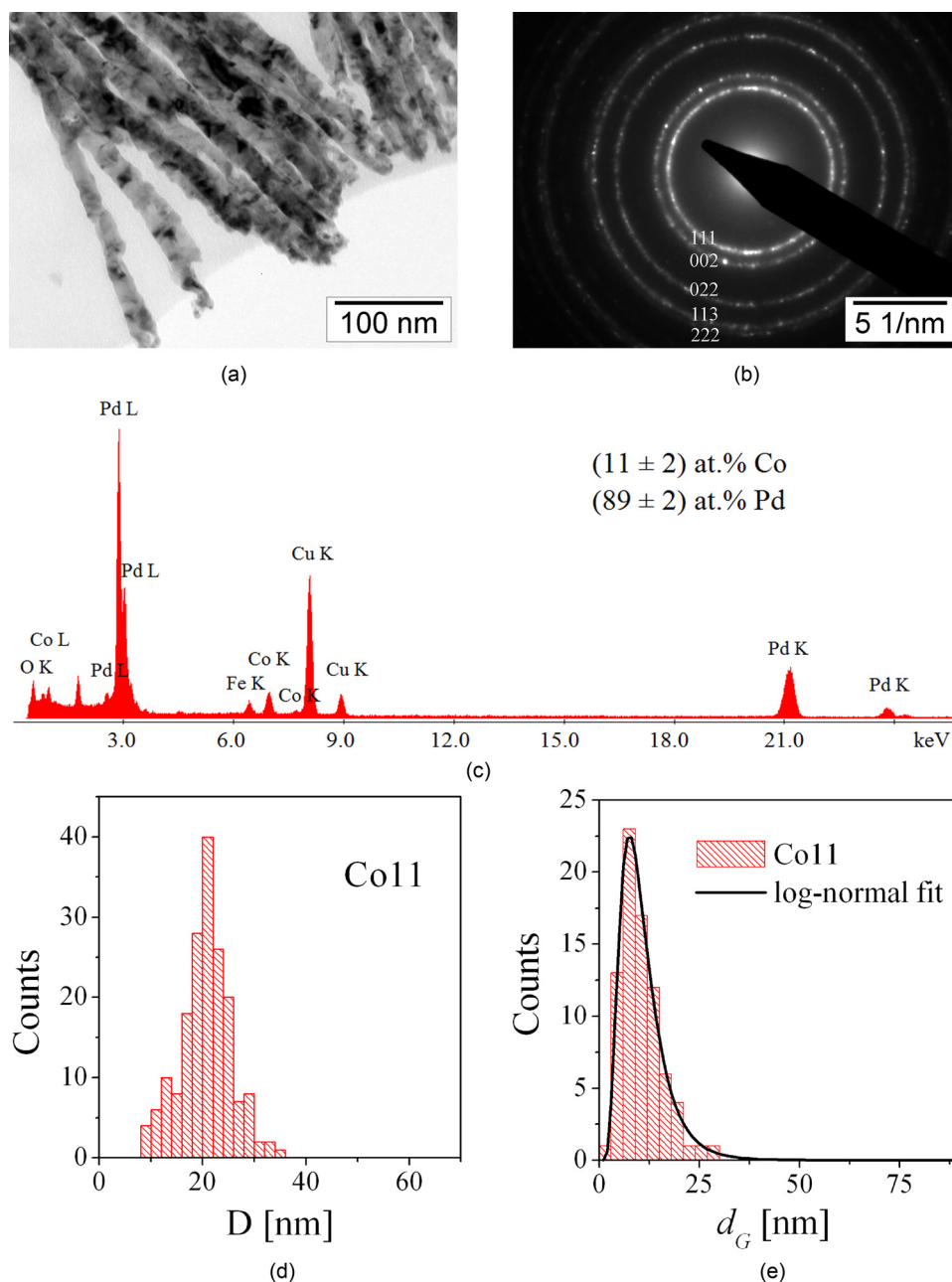


FIG. 5. (a) Bright field (BF) TEM micrograph of Co11 polycrystalline nanowires. (b) Electron diffraction pattern, (c) EDS spectrum, (d) diameter  $D$ , and (e) grain size  $d_G$  histograms, resulting from TEM data.

In all the samples, the coercive field is notably lower than that predicted by shape anisotropy effects, partially due to the granular structure of the wires, their irregular surfaces, and to the fact that the condition of a single anisotropy axis, parallel to the wire axis, may not be fulfilled. In addition, *local* conditions in the nucleation volume become relevant in the competition between shape, inter-wire interaction, and magnetocrystalline anisotropies.

In Co and Co-rich samples, the leading contribution to the coercivity arises from shape anisotropy at all temperatures, whereas in arrays with Pd contents above 45 at. %, the magnetocrystalline anisotropy becomes important, specially at low temperature. This phenomenon is likely to explain the observed dependence of coercive field on temperature shown

in Figure 7(a). At room temperature, the gradual softening observed as the Co content diminishes may be attributed to lower shape anisotropy.

At small Co concentrations, the increase in coercivity at low temperature can therefore, be explained by changes from a soft nucleation and reversion mechanism, governed by the competition between magnetostatic and exchange energies, to a harder one, where the spin configurations are determined by the competition among magnetocrystalline and exchange energies.

Bran *et al.*<sup>26</sup> report similar hardening effects in hexagonally ordered *bcc*  $\text{Fe}_{28}\text{Co}_{67}\text{Cu}_5$  nanowires (18–27 nm diameter), connected with a partial reduction of the saturation magnetization after annealing at 500 °C. They found that the



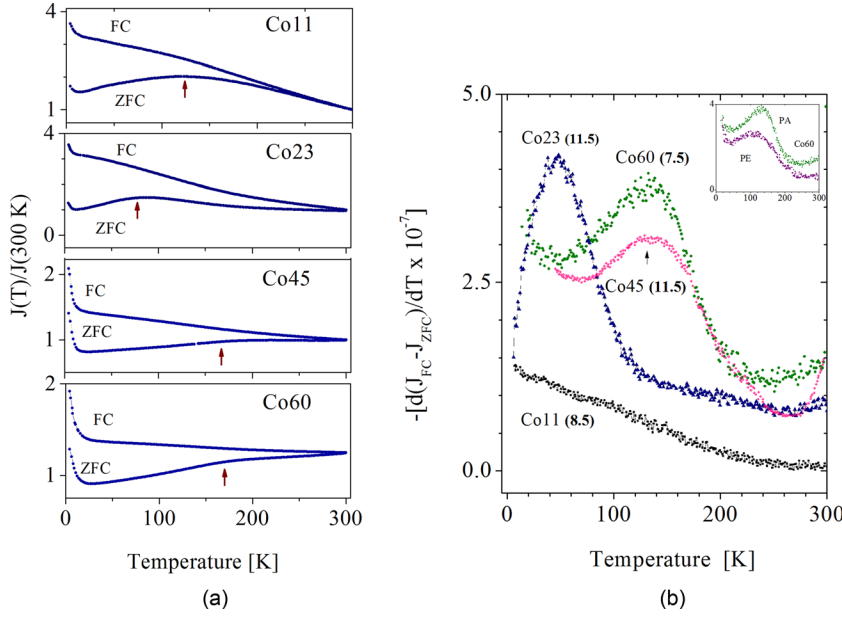


FIG. 6. (a) Relative polarization vs. temperature curves measured following the ZFC-FC protocols with an applied field of 10 mT. All the nanowire arrays show a rather wide maximum below 300 K (arrows). (b) Blocking temperature distributions corresponding to nanowire arrays in (a). The peak temperature increases with the Co content and the mean grain size, but is little sensitive to the wire diameter. Curves in the inset correspond to sample Co60 with the applied field parallel (PA) and perpendicular (PE) to the wire long axis.

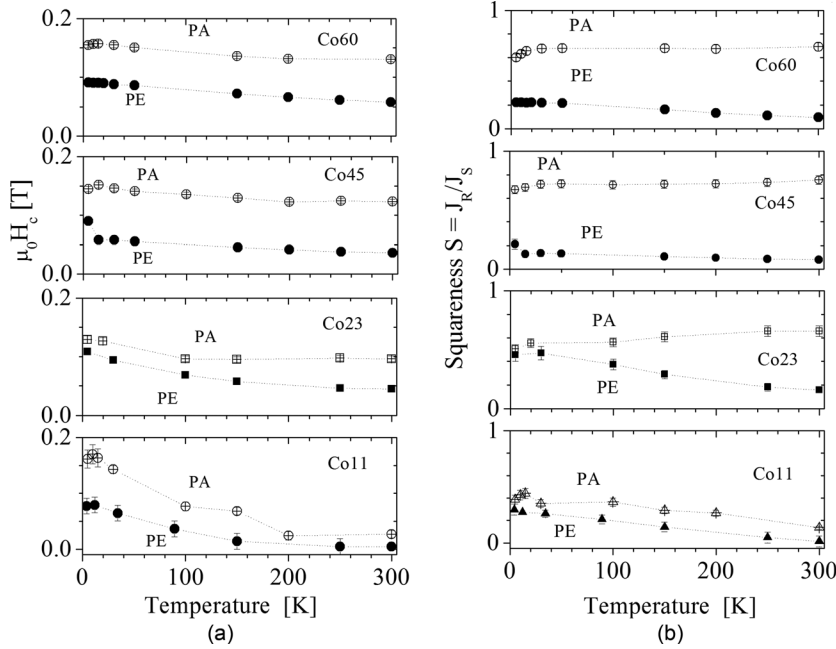


FIG. 7. (a) Temperature dependence of coercivity in Co60, Co45, Co23, and Co11 nanowire arrays. PA and PE indicate that the magnitude is measured with the magnetic field applied parallel or perpendicular to the nanowire long axis. (b) Squareness vs. temperature for nanowire arrays in (a).

TABLE II. Magnetic parameters and magnetic lengths corresponding to the different samples, at two temperatures: 4 K and 300 K. Magnetic lengths as the exchange length  $L_{ex} (= \sqrt{2A\mu_0/J_S^2} = \delta_w^*)$ , the coherence diameter  $D_{coh} (= 7.3\sqrt{\mu_0 A/J_S^2})$  (Ref. 3) and the domain wall parameter  $\delta_w (= \sqrt{A/K_C}) \delta$  estimated using the parameters' values in the table are also included.

Sample	$T$ (K)	$K_C$ $10^{5,a}$ (J/m <sup>3</sup> )	$J_S$ <sup>b</sup> (T)	$\lambda_S$ $10^{-6,a}$ (nm)	$\delta_w$ (nm)	$E$ (GPa)	$L_{ex}$ (nm)	$D_{coh}$ (nm)
Co100	300	-0.62	1.81	-55	15.5	209	5.6	18
	4	-0.74	1.90	-40	14.2		5.2	16
Co60	300	-0.26	1.24	-10	18.6	174	7.3	20
	4	-0.32	1.32	-80	16.7		6.9	19
Co45	300	-0.40	1.04	-51	12.2	161	7.8	21
	4	-0.45	1.09	-94	11.5		7.2	19.5
Co23	300	-0.17	0.75	-140	14.2	141	9.3	22
	4	-0.56	0.78	-169	7.8		7.1	19.4
Co11	300	-0.06	0.45	-50	16.6	131	11.7	25
	4	-0.57	0.47	-125	5.4		9.4	22

<sup>a</sup>References 22 and 23.

<sup>b</sup>Reference 21.

TABLE III. Upper bounds of the different contributions to the effective anisotropy field in the arrays: the magnetocrystalline  $\mu_0 H_K$  anisotropy field, the shape anisotropy field  $\mu_0 H_{sh}$ , the magnetoelastic anisotropy field  $\mu_0 H_\lambda$ . The demagnetizing field,  $\mu_0 H_{dip}$  ( $= -PJ_S$ ) is estimated with a mean field approximation.<sup>10</sup>

Sample	$T$ (K)	$\mu_0 H_{dip}$ (mT)	$\mu_0 H_K$ (mT)	$\mu_0 H_\lambda$ (mT)	$\mu_0 H_{sh}$ (mT)	$\mu_0 H_{C-PA}$ (mT)	$\mu_0 H_{C-PE}$ (mT)
Co100	300	-182	85.6	-1	887	167.5	24
	4		52.9	-20	926	180.5	42
Co60	300	-124	52.7	-1.1	604	132	59
	4		60.9	-48	643	158	93
Co45	300	-104	33.8	-1.2	506	123	38
	4		66.8	-63	531	145	90
Co23	300	-75	40.2	-4	365	95	45
	4		174	-139	380	127	109
Co11	300	-45	7.8	-2.2	219	26	5
	4		305	-159	229	167.5	77

observed hardening aroused from the transition from vortex (softer) to transverse (harder) domain-wall reversal modes as the shape anisotropy reduced.

In arrays of Co nanowires with varying length, Vivas *et al.*<sup>27</sup> reported decreasing coercivity values with the increase in the nanowire aspect ratio, in contrast to the behavior expected from the shape anisotropy. The measurements were interpreted considering the change in the dominant crystalline phase detected, from *fcc* cubic to *hcp* hexagonal with (100) texture, in small and high aspect ratio nanowires, respectively. The experimental evolution of the coercivity with the nanowires length is probably due to the variation in their crystalline structure.

Vivas *et al.*<sup>28</sup> also considered arrays of Co nanopillars with 120 nm height and variable diameter, which reported crucial changes of hysteresis loops when the diameter was increased (decreasing  $a_r$  and so the longitudinal shape anisotropy). They also showed a change in the reversal mode with the increased diameter, from vortex propagation to curling, when the field is applied parallel to the nanopillar axis. When applied perpendicularly, the shift was from coherent rotation to curling. The authors explained the transitions based on changes of both magnetocrystalline and shape anisotropies as well as on the interactions between nanopillars.

In the present case of polycrystalline *fcc* Co(Pd) nanowires, no changes in the crystalline structure with composition nor with the wire geometry were observed. However, nucleation localization volumes and local spin configurations within them are expected to be determined by both, the exchange energy and the dominant term between magnetostatic and magnetocrystalline energy.

#### D. Localized nucleation modes

These strong temperature and composition dependences of the magnetocrystalline energy density induce large changes in the localization length of the nucleation modes.<sup>2,3</sup> Figure 8 illustrates the distribution of the different arrays investigated in a Skomski-map [Fig. 2 in Ref. 2] at 300 K (circles) and at 4 K (triangles). In this map, the abscise values  $D/d_G$  only depend on the wire morphology, and they indicate to what extent the wires are polycrystalline. In the ordinate, the mean grain size  $d_G$  in the wire is compared to the relevant magnetic correlation length  $\delta_w$  or  $\delta_w^*$  depending on

which anisotropy, either crystalline or magnetostatic, determines the local spin configuration. This magnitude indicates whether the nucleation mode is cooperative or non-cooperative. In Co and Co60 nanowires with  $\delta_w^*/d_G < 1$ , nucleation events involve a few or individual grains, undergoing little or non-cooperative modes (regions II and V). In the other arrays with compositions above 55 at. % of Pd and small grain size  $\delta_w/d_G > 1$ , the exchange interaction ensures a cooperative behavior at room temperature (regions III and IV).

Figure 8 also shows that Co-rich arrays practically remain in the same nucleation localization regime (minor displacements in the map) when temperature lowers to 4 K. Contrarily, Pd-rich wires largely move from the cooperative regimes at room temperature to harder non-cooperative ones at 4 K.

These facts are also consistent with the experimental observation of increasing coercivity and relative remanence in arrays with low Co contents, as the temperature reduces below 100 K.

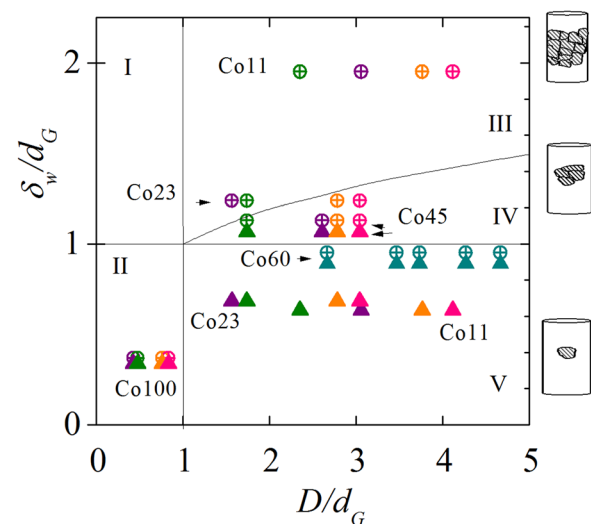


FIG. 8. Nanowire arrays investigated in a Skomski-map<sup>2</sup> at 300 K (circles) and at 4 K (triangles). Regions correspond to nucleation modes: (I) one dimensional, cooperative; (II) one dimensional, non-cooperative; (III) quasi-one-dimensional, cooperative; (IV) three-dimensional, cooperative, and (V) three-dimensional non-cooperative.

#### IV. CONCLUSIONS

Co-Pd nanowires with different compositions and diameters (18 nm–35 nm) have been produced by AC electrodeposition into the hexagonally arranged pores of a self-assembled alumina template. The nanowires obtained by this AC method are nanocrystalline, with randomly oriented equiaxed grains of mean sizes between 7 nm and 12 nm (smaller than the wire diameter). No correlation could be established between grain size and the alloy composition or the wire diameter.

The nanowire arrays are ferromagnetic in the whole temperature range (4 K–300 K). Moreover, they all exhibit an easy magnetization axis parallel to the long wire axis (out of the substrate plane) and a hard direction perpendicular to the nanowire length, with no crossover in the temperature ranges investigated.

The coercive field and the relative remanence of the nanowire arrays increase along with the Co content in the alloy. As Pd-rich wires have very small grains, the coercive fields and the relative remanences (in PA and PE configurations) largely increase when cooling below 100 K. These effects arise from a strong temperature and composition dependences of the magnetocrystalline energy density in Co-Pd alloys near 10–20 at. % Co. Due to this drastic increase in the magnetocrystalline anisotropy, a reduction of the localization length takes place promoting harder non-cooperative nucleation modes.

#### ACKNOWLEDGMENTS

The authors wish to thank FONCyT, SECyT-UNC, and CONICET Argentina for the financial support given to this work.

- <sup>1</sup>R. Hertel, “Computational micromagnetism of magnetization processes in nickel nanowires,” *J. Magn. Magn. Mater.* **249**(1–2), 251–256 (2002).
- <sup>2</sup>R. Skomski, H. Zeng, M. Zheng, and D. J. Sellmyer, “Magnetic localization in transition-metal nanowires,” *Phys. Rev. B* **62**(6), 3900–3904 (2000).
- <sup>3</sup>R. Skomski, H. Zeng, and D. J. Sellmyer, “Incoherent magnetization reversal in nanowires,” *J. Magn. Magn. Mater.* **249**, 175–180 (2002).
- <sup>4</sup>R. Skomski, “Exact nucleation modes in arrays of magnetic particles,” *J. Appl. Phys.* **91**, 7053 (2002).
- <sup>5</sup>I. S. Jacobs and C. P. Bean, “An approach to elongated fine-particle magnets,” *Phys. Rev.* **100**(4), 1060–1067 (1955).
- <sup>6</sup>A. Aharoni, “Angular dependence of nucleation by curling in a prolate spheroid,” *J. Appl. Phys.* **82**, 1281 (1997).
- <sup>7</sup>P. Landeros, S. Allende, J. Escrig, E. Salcedo, D. Altbir, and E. E. Vogel, “Reversal modes in magnetic nanotubes,” *Appl. Phys. Lett.* **90**, 102501 (2007).
- <sup>8</sup>R. Lavin, J. C. Denardin, J. Escrig, D. Altbir, A. Cortés, and H. Gómez, “Angular dependence of magnetic properties in Ni nanowire arrays,” *J. Appl. Phys.* **106**, 103903 (2009).
- <sup>9</sup>R. Lavin, J. C. Denardin, A. P. Espejo, A. Cortés, and H. Gómez, “Magnetic properties of arrays of nanowires: Anisotropy, interactions, and reversal modes,” *J. Appl. Phys.* **107**, 09B504 (2010).
- <sup>10</sup>A. Encinas-Oropesa, M. Demand, L. Piraux, I. Huynen, and U. Ebels, “Dipolar interactions in arrays of nickel nanowires studied by ferromagnetic resonance,” *Phys. Rev. B* **63**, 104415 (2001).
- <sup>11</sup>Q. F. Zhan, J. H. Gao, Y. Q. Liang, N. L. Di, and Z. H. Cheng, “Dipolar interactions in arrays of iron nanowires studied by Mössbauer spectroscopy,” *Phys. Rev. B* **72**, 024428 (2005).
- <sup>12</sup>F. Zighem, T. Maurer, F. Ott, and G. Chaboussant, “Dipolar interactions in arrays of ferromagnetic nanowires: A micromagnetic study,” *J. Appl. Phys.* **109**, 013910 (2011).
- <sup>13</sup>O. Dmytriiev, U. A. S. Al-Jarah, P. Gangmei, V. V. Kruglyak, R. J. Hicken, B. K. Mahato, B. Rana, M. Agrawal, A. Barman, M. M. átéfi-Tempfli, L. Piraux, and S. M. átéfi-Tempfli, “Static and dynamic magnetic properties of densely packed magnetic nanowire arrays,” *Phys. Rev. B* **87**, 174429 (2013).
- <sup>14</sup>J.-E. Wegrowe, D. Kelly, A. Franck, S. E. Gilbert, and J.-Ph. Ansermet, “Magnetoresistance of ferromagnetic nanowires,” *Phys. Rev. Lett.* **82**(18), 3681–3684 (1999).
- <sup>15</sup>D. J. Sellmyer, M. Zheng, and R. Skomski, “Magnetism of Fe, Co and Ni nanowires in self-assembled arrays,” *J. Phys.: Condens. Matter* **13**, R433 (2001).
- <sup>16</sup>M. Vázquez and L. G. Vivas, “Magnetization reversal in Co-base nanowire arrays,” *Phys. Status Solidi B* **248**(10), 2368–2381 (2011).
- <sup>17</sup>H. Masuda and K. S. Fukuda, “Ordered metal nanohole arrays made by a two-step replication of honeycomb structures of anodic alumina,” *Science* **268**, 1466–1468 (1995).
- <sup>18</sup>K. Nielsch, J. Choi, K. Schwirn, R. B. Wehrspohn, and U. Gosele, “Self-ordering regimes of porous alumina: The 10% porosity rule,” *Nano Lett.* **2**, 677 (2002).
- <sup>19</sup>J. Escrig, J. Bachmann, J. Jing, M. Daub, D. Altbir, and K. Nielsch, “Crossover between two different magnetization reversal modes in arrays of iron oxide nanotubes,” *Phys. Rev. B* **77**, 214421 (2008).
- <sup>20</sup>M. Knobel, W. C. Nunes, L. M. Socolovsky, E. De Biasi, J. M. Vargas, and J. C. Denardin, “Superparamagnetism and other magnetic features in granular materials: A review on ideal and real systems,” *J. Nanosci. Nanotechnol.* **8**, 2836–2857 (2008).
- <sup>21</sup>R. M. Bozorth, P. A. Wolff, D. D. Davis, V. B. Compton, and J. H. Wkrnick, “Ferromagnetism in dilute solutions of cobalt in palladium,” *Phys. Rev.* **122**(4), 1157–1160 (1961).
- <sup>22</sup>J. H. Fujiwara, H. Kadomatsu, and T. Tokunaga, “Magnetocrystalline anisotropy and magnetostriction of Pd-Co alloys,” *J. Magn. Magn. Mater.* **31–34**, 809–810 (1983).
- <sup>23</sup>H. Takahashi, S. Tsunashima, S. Iwata, and S. Uchiyama, “Measurement of magnetostriction constants in polycrystalline alloy and multilayer films of PdCo and PtCo,” *J. Magn. Magn. Mater.* **126**, 282–284 (1993).
- <sup>24</sup>R. C. O’Handley, *Modern Magnetic Materials: Principles and Applications* (John Wiley and Sons, New York, 2000).
- <sup>25</sup>J. Sánchez-Barriga, M. Lucas, F. Radu, E. Martin, M. Multigner, P. Marin, A. Hernando, and G. Rivero, “Interplay between the magnetic anisotropy contributions of cobalt nanowires,” *Phys. Rev. B* **80**, 184424 (2009).
- <sup>26</sup>C. Bran, Yu. P. Ivanov, J. Garcia, R. P. del Real, V. M. Prida, O. Chubykalo-Fesenko, and M. Vázquez, “Tuning the magnetization reversal process of FeCoCu nanowire arrays by thermal annealing,” *J. Appl. Phys.* **114**, 043908 (2013).
- <sup>27</sup>L. G. Vivas, R. Yanes, O. Chubykalo-Fesenko, and M. Vázquez, “Coercivity of ordered arrays of magnetic Co nanowires with controlled variable lengths,” *Appl. Phys. Lett.* **98**, 232507 (2011).
- <sup>28</sup>L. G. Vivas, Yu. P. Ivanov, D. G. Trabada, M. P. Proença, O. Chubykalo-Fesenko, and M. Vázquez, “Magnetic properties of Co nanopillar arrays prepared from alumina templates,” *Nanotechnology* **24**, 105703 (2013).